Maksymilian Klimontowicz[1], Amer Al-Hinai[1,2,*], Jimmy C.-H. Peng[1]

J. Electrical Systems 12-1 (2016): 68-84

Regular paper

Optimal LFC SMC for three – area power system with high penetration of PV

Electrical power systems are subjected to new trends appearing in grid structuring, electrical power sources, new control strategies, etc. The introduction of inverter-based distributed energy resources to replace conventional synchronous machines depletes the mechanical inertia, and causing the system to become more sensitive to disturbances. This paper proposed a simple and reliable solution to assure sufficient frequency stability of electrical power systems when subjected to high penetration of decoupled distributed generation. To achieve this, a decentralized sliding mode control was designed to operate as a compensator for conventional load frequency controllers. Subsequently, PV farms and battery energy storage systems were interconnected. Simulated network under different configurations were conducted using MATLAB.

Keywords: load frequency control, sliding mode control, distributed energy resources

Article history: Received 15 September 2015, Accepted 16 February 2016

1. Introduction

Frequency deviation is defined as the difference between current system frequency and the scheduled value [1], [2]. According to the European Network of Transmission System Operators for Electricity (ENTSO-E) regulation policy, [2], the grid frequency is allowed to swing between ±180 mHz or 200 mHz for a system with and without load self-regulation, respectively. In order to reach quasi-steady-state, the grid will continuously drive the integral of frequency deviation trajectory to zero within a predefined timeframe. Such control action is essential for electronic devices, which calculate time based on power supplied frequency.

Modern power systems regulatory policies subdivide frequency regulation into three parts: primary, secondary, and tertiary control. Primary control is an intrinsic feature of every power unit. It is responsible for providing local responses to mitigate encountered disturbances. The amount of control effort is proportional to the rating of each device, and does not necessary resolve frequency deviations.

The aim of the secondary frequency regulation is to maintain the frequency and/or the scheduled power flows in tie-lines. The input signal to the secondary controller is known as the Area Control Error (ACE), which is a linear combination of frequency and tie-line power deviations. Broader descriptions of modes, states, and organization of the secondary regulation can be referred to [2] and [3]. Usually PI type controller is utilized in each assigned control area in the system [1, 2].

In the European interconnected electrical power system, tertiary control or tertiary reserves are divided into: directly activated and schedule activated. Directly activated can

* Corresponding author: Amer Al-Hinai, alhinai@masdar.ac.ae
[1] Masdar Institute of Science and Technology, iEnergy Center, P.O. Box 54224, Abu Dhabi, UAE
[2] Sultan Qaboos University, Electrical & Computer Engineering, PO Box 33, PC 123, Alkhoud, Oman

be individually adjusted apart from the schedule. While schedule activated are related to load dispatch, which is the contracted power output schedule throughout the day.

In the literature, improvements in frequency regulation algorithms have been widely studied. A combination of robust and adaptive control methods was published in [4] to regulate frequency with parametric uncertainties ranging from 30% to 50% of their nominal values. Meanwhile, frequency control in an isolated system by means of small hydro power plant with multiple pipe flow control and a thyristor-controlled heater was proposed [5]. Results demonstrated that it is possible to control frequency in an effective manner. Authors of [6] proposed Active Disturbance Rejection Control (ARDC) for a three-area system model. ARDC utilized extended state observer approach to cancel the generalized disturbance effect in every control area. Under certain conditions, the LFC system is able to differentiate between units with and without secondary control loop in each area. This allowed [5] to perform better in terms of robustness than PI controller utilized as benchmark.

Linear Matrix Inequality based control was proposed in [7] and [8]. In [7], authors developed a robust full order controller to deal with time delays in communication network, while [8] utilized a H_∞ based controller and adopted a Genetic Algorithm Linear Matrix Inequality (GALMI) to tune the PI controller. Comparisons between both methods show that properly optimized GALMI PI controller can match H_∞ based controller performance while PI has simpler structure in comparison to high order H_∞ controller.

Moreover, many optimization algorithms were utilized to design secondary frequency control systems. Authors of [9] utilized integrated square method (ISE) to obtain a gain settings for control gains with and without presence of battery energy storage systems (BESS). Whereas, author of [10] designed controllers using Multidimensional Unconstrained Nonlinear Minimization (MUNM) and Particle Swarm Optimization (PSO). PSO is a very popular and effective optimization method. It has been utilized by many researcher [11, 12, 13]. Another popular heuristic-based optimization technique is Genetic Algorithm (GA) [14]. Publications like [6] and [8] implemented genetic algorithm linear matrix inequality tuning to find the most optimal of control gains. Extensions in terms of considering Distributed Energy Resources (DERs) have also been studied [17, 18, 19]. In [17], high wind farm penetration was considered. Subsequently, an observer to reject the output power fluctuations was designed. On the other hand, [18] and [19] installed BESS and proved that such system configuration can perform better than without BESS.

In recent years, sliding mode controllers were proposed in the secondary frequency controllers. A good example of a classical SMC is given in [14] and [20]. Authors of [14] considers linear surface SMC applied to generalized power system model. In contrast, [21] developed a PI sliding surface SMC to assure good LFC performance for matched and unmatched uncertainties in the model. However, the presence of intermittent generations from DERs such as PV impose nonlinearity to LFC model. The existing literature have not consider a generalized power system model with the influence of large penetration of PV system.

The objective of this work is to improve existing LFC methods by adding a compensation procedure to the system. This task is fulfilled by means of a sliding mode based compensator, where its parameters are chosen using GA. The second objective of this work is to provide a compact solution for frequency regulation when electrical power system is affected by large penetration of PV accompanied with BESS. The proposed methodology is applied to a three areas interconnected AGC model. In order to demonstrate

the effectiveness of the proposed controller, the dynamical behavior of the proposed controller is compared to conventional PI and PID controllers optimally designed by GA.

The organization of this paper is as follows. An overview of the generalized three-area power system model including the BESS and PV model are presented in Section 3 followed by a review of the SMC theory in Section 4. Simulations results and comparisons with the conventional LFC optimally designed by GA are presented in Section 5. Finally, conclusions are drawn in Section 6.

2. Notations

The notations used throughout the paper are stated below.

Indexes:

i	electrical area index

Constants:

K_{B_i}	Bias constant
K_{E_i}	Integral gain
R_i	Droop control
T_{G_i}	Governor time constant
T_{T_i}	Turbine time constant
T_{P_i}	Generator time constant
$K_{S_{ij}}$	Synchronizing torque
I_{sat}	PV panel saturation current
I_{SC}	PV short circuit current
A	Diode ideality factor
R_{sh}	PV panel shunt resistance
R_s	PV panel series resistance
T	Junction temperature
K	Boltzmann's constant
q	Electron charge
K_I	Junction short circuit temperature coefficient
I_{dsc}	Dark saturation current

Variables:

ACE_i	Area Control Error
ΔE_i	Speed reference deviation
ΔX_{g_i}	Valve position deviation
ΔP_{g_i}	Turbine power output deviation
Δf_i	Frequency deviation
$\Delta\delta_i$	Power angle deviation
σ_i	Sliding surface
x_i	State vector
A_i	Model matrix
B_i	Control matrix

P_i Vector of sliding surface polynomial coefficients
K_i SMC gain
V_0 PV output voltage
I_0 PV output current
I_g PV generated current
P_0 PV output power
I_{rr} Irradiance

3. Generalized three - area power system model

A generalized power system model is implemented for the purpose of LFC studies. The concept originated from [1], and the control diagram of one area is illustrated in Fig.1.

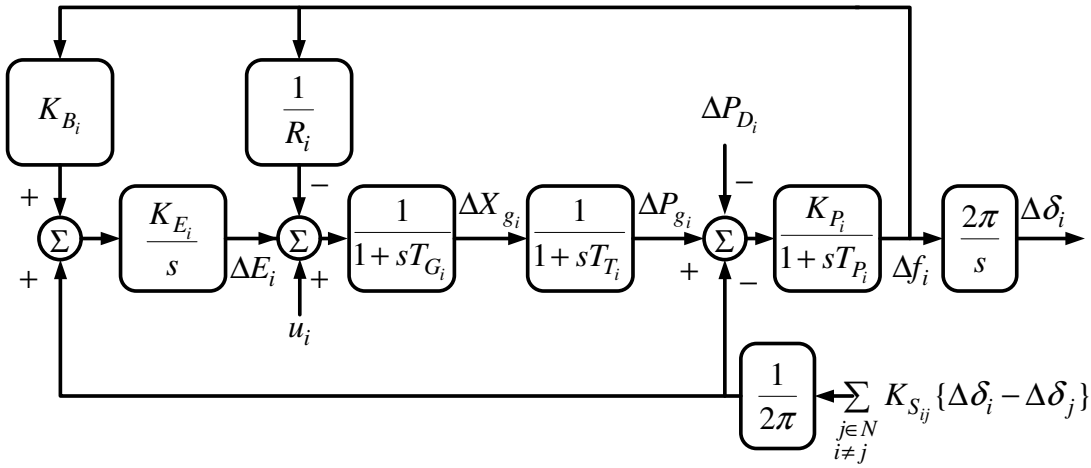

Fig.1. Model of single area LFC scheme.

Each area consists of a governor and turbine with time constants $T_{G\,i}$ and $T_{T\,i}$, respectively. The primary frequency control loop is equipped with a droop R. The generator and load models have a time constant of $T_{P\,i}$ and gain $K_{P\,i}$, respectively. While secondary control loop includes LFC regulator with gain $K_{E\,i}$, bias $K_{B\,i}$ and feedback from another control areas multiplied with $K_{S_{ij}}$ which represents a synchronizing torque between areas. The model parameters of the generalized three-area power system utilized for the purpose of simulation are presented in Table 1.

Table 1: Data of Three – Area System

Area	1	2	3
$T_{P\,i}$	20	25	20
$K_{P\,i}$	120	112.5	115
$T_{T\,i}$	0.3	0.33	0.35
$T_{G\,i}$	0.008	0.072	0.07
R_i	2.4	2.7	2.5
$K_{B\,i}$	0.41	0.37	0.4
$K_{S_{ij}}$	0.55	0.55	0.65
	0.65	0.545	0.545

The conventional control gains are found by means of GA set as in Table 2 with a fitness

function outlined in equation (1) and constraints shown in (c.1~5). Documents [26, 27] defines constraints over frequency deviations in synchronized European and North American power systems respectively. However, for the purpose of this work, the problem is relaxed from some constraints and the system reaches desired performance. Results of GA search are shown in Table 3, while GA optimization process flow chart is presented in Fig.2. According to GA theory which has been delineated in many resources e.g. [25], GA search starts with initial population which can be an input or generated randomly by the program within defined bounds. Subsequently, the initial populations' performance is assessed by the fitness function. If any of the proposed solutions satisfies stopping criteria, then algorithm stops. On the other hand, if the system performance varies significantly or the constraints are not satisfied then GA calculates new population based on three mainly utilized operators, which are: mutations, crossovers and selections. When the new population is formed then fitness evaluation is processed again.

$$\min \sum_{i=1}^{3} \int |ACE_i| \tag{1}$$

Subject to:

a) Steady state deviation of frequency according to [26]

$$|\Delta f_i| < 180\ mHz\ for\ steady\ state\ operation \tag{c.1}$$

b) Dynamic deviation of frequency according to [26]

$$|\Delta f_i| < 800\ mHz\ for\ steady\ dynamic\ operation \tag{c.2}$$

c) Constraints over conventional control gains

$$0 < k_{P_i}, k_{I_i}, k_{D_i} < 10 \tag{c.3}$$

d) Constraints over SMC control gains

$$0 < K_i < 1 \tag{c.4}$$

e) Constraints over SMC polynomial coefficients

$$0 < P_i < 3 \tag{c.5}$$

In this paper, DERs are modelled as PV panels described by equations (2)~(5). The model represents the output current, output power, generated current, and saturation current, respectively. This model is iteratively solved to obtain active power output from one panel and then scaled for the purpose of full electrical power system size. The solution for irradiances from $600 - 700\ W/m^2$ is presented in Table 5.

Table 2: GA optimization parameters

No of generation	*600*
Population size	*100*
Mutation function	*Constraint dependent*
Mutation rate	*0.01*
Crossover function	*Scattered*
Crossover fraction	*0.8*
Selection function	*Stochastic*
Reproduction rate	5
Function tolerance	*1e-6*
Stall generations	*50*

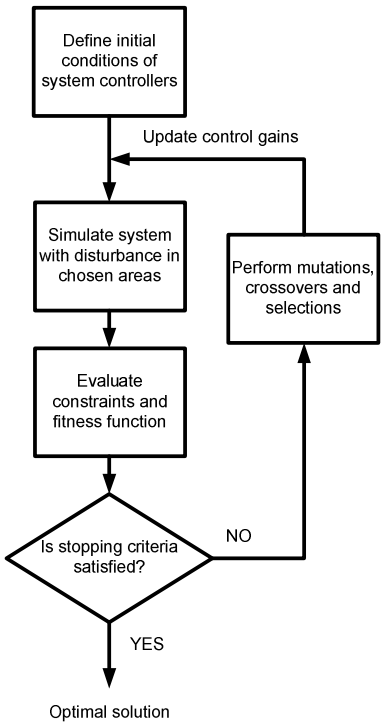

Fig.2. GA optimization flowchart.

Table 3: Optimal Control Gains For Conventional Controllers

Area		1	2	3
Gains	P	0.011	0.0225	0.014
	I	0.3377	0.4766	0.3675
	P	0.0438	4.0988	3.5624
	I	0.8244	5.1677	4.569
	D	0.0152	1.0419	0.7762

$$I_0 = I_g - I_{sat} * \left[e^{\frac{q(V_0+I_0R_S)}{AKT}} - 1\right] - \frac{V_0 + I_0R_s}{R_{sh}} \quad (2)$$

$$P_0 = V_0 * \left[I_g - I_{sat} * \left[e^{\frac{q(V_0+I_0R_S)}{AKT}} - 1\right] - \frac{V_0 + I_0R_s}{R_{sh}}\right] \quad (3)$$

$$I_g = [I_{SC} + K_I(T - 25)]\frac{Irr}{100} \tag{4}$$

$$I_{sat} = I_{dsc}\left[e^{\frac{qV}{KT}} - 1\right] \tag{5}$$

Here I_0 and V_0 are the output current and voltage. I_g and I_{sat} are the generated current under given insolation and reverse saturation current, while q and K are electron charge and Boltzmann's constant. A and T are ideality factor and module temperature and R_S and R_{sh} are series and shunt resistances. I_{sc}, I_{dsc}, K_I and I_{rr} are short circuit current, dark saturation current, short circuit temperature coefficient and insolation. Typical PV panel parameters are presented in Table 4.

Table 4: PV panel parameters

q	$1.6 * 10^{-19}$
A	1.5
k	$5.67 * 10^{-8}$
T	$273.15 + 25$
I_{sc}	8.1
I_{dsc}	$1 * 10^{-10}$
R_s	1.3
R_{sh}	1000

It is assumed that batteries are equally distributed within the system. The battery model is shown in Fig.3. Here, $K_{BESS} = 1.8$ and $T_{BESS} = 0.1s$, more details can be found in [19]. The limits $\pm P_b$ are specified by manufacturer, for example in the case of fast ABB energy management systems (EMS) such limit is 10MW [22]. The maximum power output from battery has to be reasonably sufficient to influence transient state within the system.

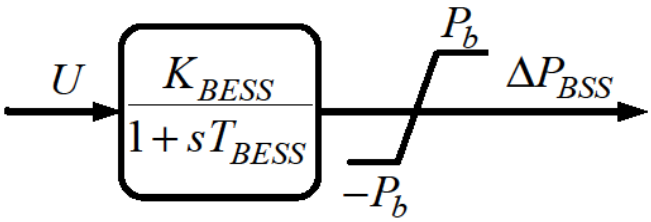

Fig.3. BESS model.

Input U to the battery energy storage system is ACE signal from local area, while the battery output signal ΔP_{BESS} is added as a change in the BESS output power to ΔP_{G_i}. At the same time the change in output power from PV panels is added to the disturbance and finally we end up with the node equation (6).

$$\Delta P_{G_i} - \Delta P_0 - \Delta P_{D_i} + \Delta P_{BESS_i} = \Delta P_{mech} - \frac{1}{2\pi}\sum_{\substack{j\in N \\ i\neq j}} K_{S_{ij}}\{\Delta\delta_i - \Delta\delta_j\} \tag{6}$$

Table 5: Solution to the PV Model

Insolation [W/m2]	P [W]	Insolation [W/m2]	P [W]
600	144.0564	650	156.2790
605	145.2786	655	157.5013
610	146.5009	660	158.7235
615	147.7232	665	159.9458
620	148.9454	670	161.1681
625	150.1677	675	162.3903
630	151.3900	680	163.6126
635	152.6122	685	164.8349
640	153.8345	690	166.0571
645	155.0568	695	167.2794

4. Sliding Mode Control - Design

Sliding Mode Control evolved from Variable Structure Systems (VSS). The basic idea of VSS is clearly presented in [23]. SMC consists of two major parts sliding surface and control law. Ideal sliding mode can be divided into two phases, which consists of the reaching phase and sliding phase. Normally, a system starts outside the sliding surface so control law should drive the system in the direction of siding surface. Then after system is already on sliding surface, it should stay on it thereafter. The second part of the system motion is called sliding phase.

In the case of the three-area generalized power system model, it is assumed that all states can be measured and are available so the observer based SMC is not indispensable. SMC is utilized as compensator to conventional secondary loop controller and occupies input u_i in Fig.1. to apply control signal. For the purpose of this work a linear sliding surface is considered. The sliding surface is given as multiplication of state vector x_i and polynomial coefficients vector P_i as in equation (7). While control law u_i is chosen as a combination of the proportional and nonlinear portion as in equation (8), where K_i is control gain and A_i and B_i are respectively system matrix and control matrix from the state-space model related to i^{th} area of the power system.

$$\sigma(x) = P_i^T * A_i x_i \tag{7}$$

$$u_i = -\frac{P_i^T * A_i x_i}{P_i^T B_i} - \frac{K_i}{P_i^T B_i}\text{sign}(\sigma_i(x_i)) \tag{8}$$

As described in [24], both (10) and (11) have to be fulfilled to provide asymptotic stability of the system. This is equivalent to the fulfillment of the second Lyapunov law for a chosen candidate function presented in equation (9).

$$V_i = \frac{1}{2}\sigma_i^2(x_i) \tag{9}$$

$$\lim_{|\sigma|\to\infty} V_i(x) = \infty \tag{10}$$

$$V_i(x)\dot{V}_i(x) \le 0 \tag{11}$$

$$\dot{V}_i(x) = \dot{\sigma(x)} * \sigma(x) = P_i^T x_i * P_i^T \dot{x}_\iota = P_i^T x_i * P_i^T [P_i^T * A_i x_i + P_i^T * B_i u_i] =$$
$$= P_i^T x_i * P_i^T \left[P_i^T * A_i x_i - P_i^T * A_i x_i + K_i sign\left(\sigma_i(x_i)\right)\right] =$$
$$= -P_i^T x_i * K_i sign\left(\sigma_i(x_i)\right) = -\sigma_i(x_i) * K_i sign\left(\sigma_i(x_i)\right)$$

First condition is apparently fulfilled. According to (9) V_i is always positive while $\dot{V}_i$ is negative, thus, (11) is also fulfilled.

SMC gain K_i and polynomial coefficients vector P_i are found by means of GA optimization process with objective function presented in equation (1). The GA results of SMC parameters are presented in Table 6.

Table 6: SMC Gains and Polynomial Coefficients

Area	1	2	3
Gain	0.6361	0.1839	0.9448
Polynomial	1.9575	0.7547	0.0759
	0.9649	0.1190	0.3371
	0.7922	0.2544	0.9392
	2.3922	0.8143	1.4619
	0.6948	0.8308	0.0844

5. Simulation Results

This section is divided into few subsections which represent different system cases. System Case 1 shows the comparison of PI, PID, and SMC equipped traditional electrical power system subjected to the disturbance in the first area. While, System Case 2 considers intermittency of the PV sources. System performance and test case details are presented in subsection 5.2. Third system case is included in subsection 5.3. It is dedicated to show the comparison of the BESS equipped power system performance when subjected to multi – disturbance scenario. Consequently, PV intermittency in the system equipped with BESS is presented in System Case 4 in subsection 5.4. While in subsection 5.5 sensitivity analysis of the system subjected to different PV intermittency penetration is illustrated.

5.1. System Case 1

This system case shows the conventional system behavior when subjected to the disturbance in a particular area. Fig.4, 5, 6 show frequency responses of different areas of the system while subjected to the disturbance $\Delta P_D = 0.005 p.u.$ applied in the first one. It is clear that SMC outperforms conventional PI and PID in terms of under and overshoot and settling time.

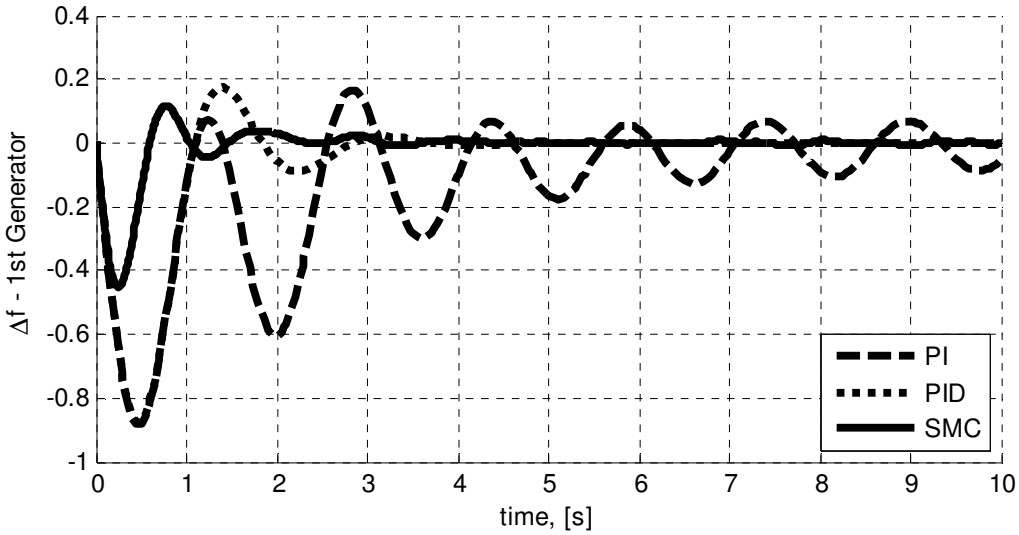

Fig.4. Frequency deviation in 1^{st} area.

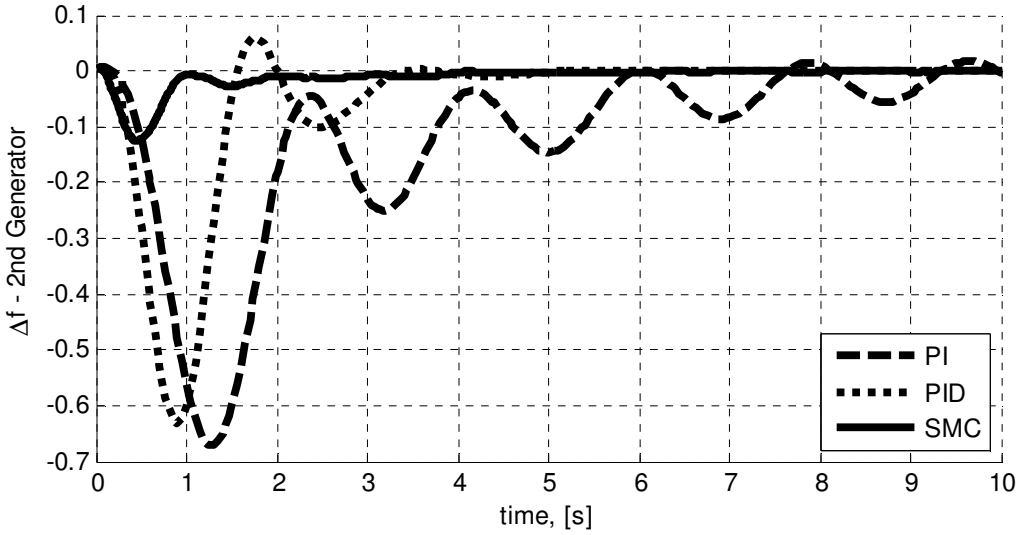

Fig.5. Frequency deviation in 2^{nd} area.

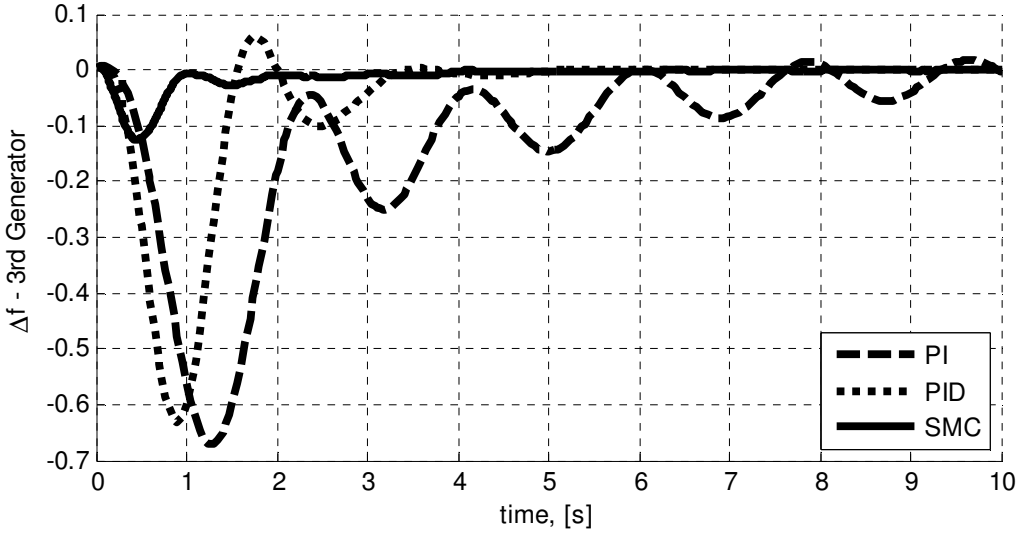

Fig.6. Frequency deviation in 3^{rd} area.

It is apparent that performance of PID and SMC are far better that PI when system does not include PV and BESS. Thus, in next simulations only PID and SMC controllers are considered. Such decision has been made because next simulations consider the electrical power system behavior affected by DERs but in the real scenario DERs can be not operational so the frequency control strategy has to be prepared for such conditions too.

5.2. System Case 2

In this test case, the system is subjected to a disturbance imposed by PV intermittency. Overall penetration of PV based sources is equal to 30% of declared load - 3.1 GW. It is also assumed that all PV plants are equally distributed within the power system. The disturbance is caused by change in insolation from $600 - 700\ W/m^2$ in 15% of panels in the first area of the system. Results are presented in Fig.7, Fig.8 and Fig.9. It is clear that the SMC performs significantly better in terms of undershot when SMC is employed in the secondary frequency control. However, some minor chattering is visible also but its amplitude is still within the acceptable limits.

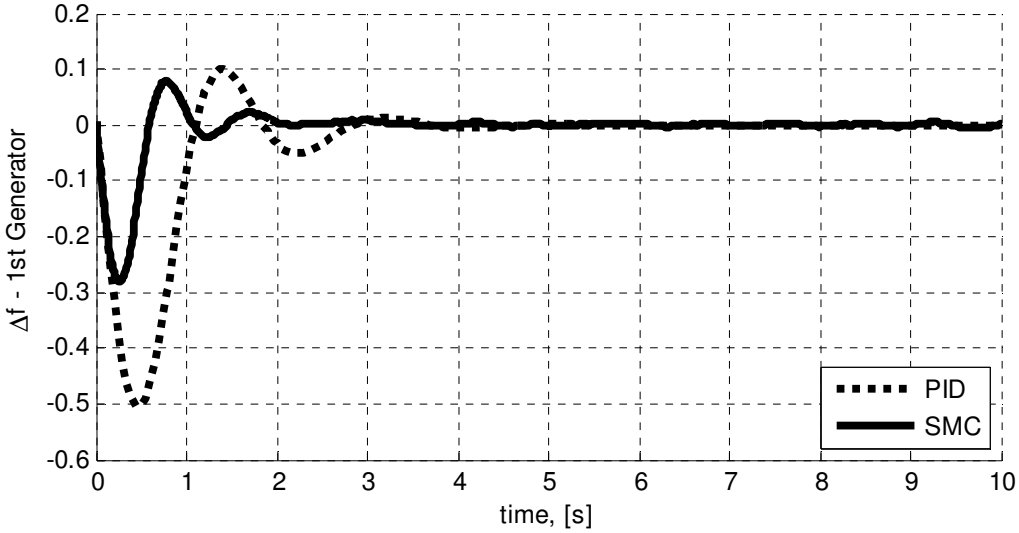

Fig.7. Frequency deviation in 1^{st} area.

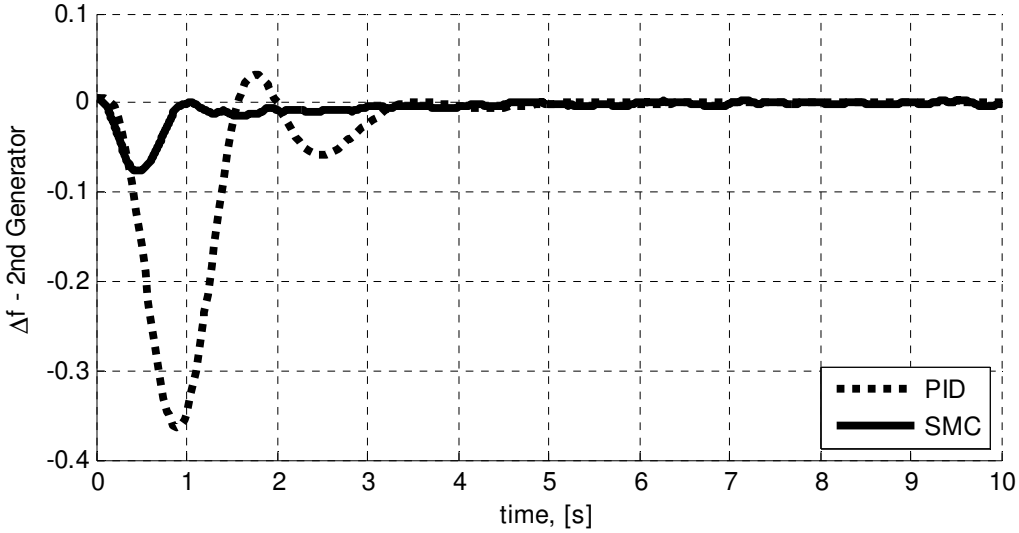

Fig.8. Frequency deviation in 2^{nd} area.

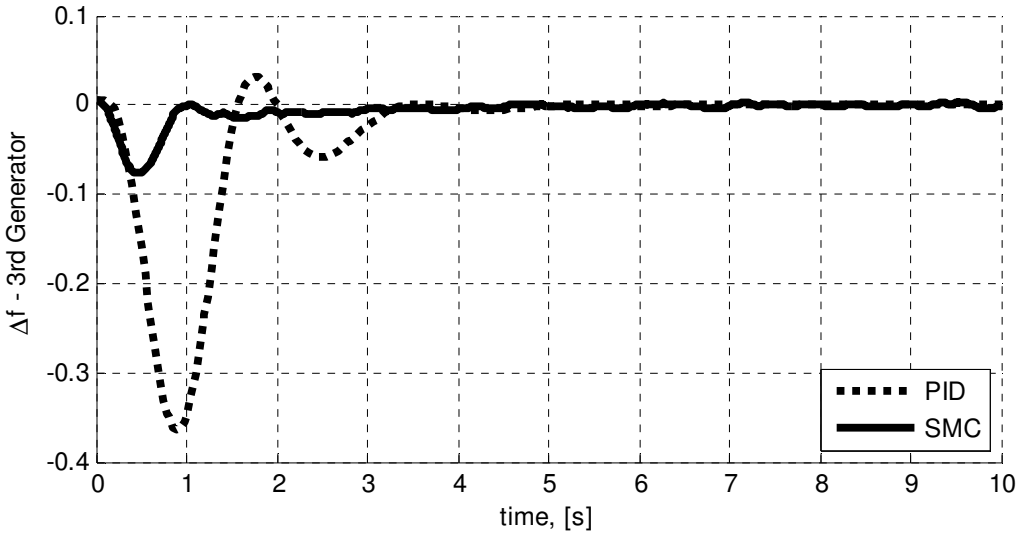

Fig.9. Frequency deviation in 3^{rd} area.

5.3. System Case 3

The third part of the simulation presents a comparative evaluations between PID and SMC performance when BESS is introduced to the system. In this case, the three-area model is subjected to multiple disturbances coming from loads in the first and the second area.

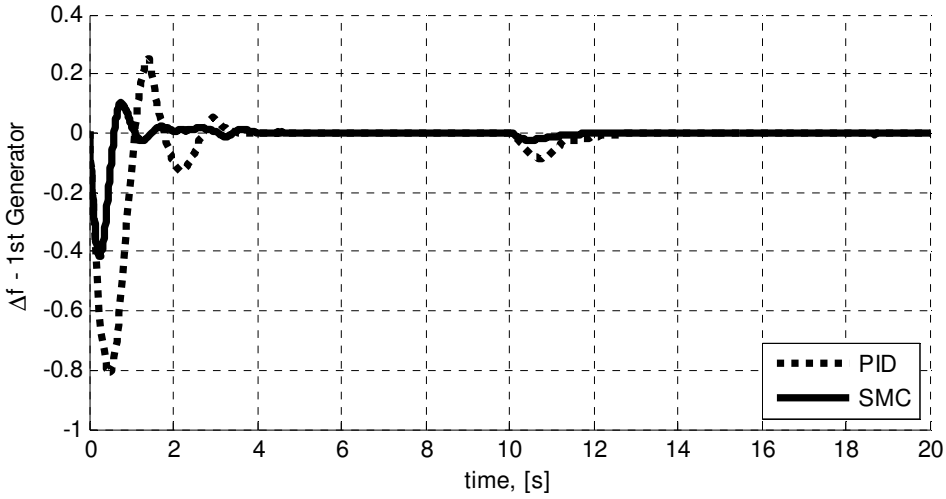

Fig.10. Frequency deviation in 1^{st} area.

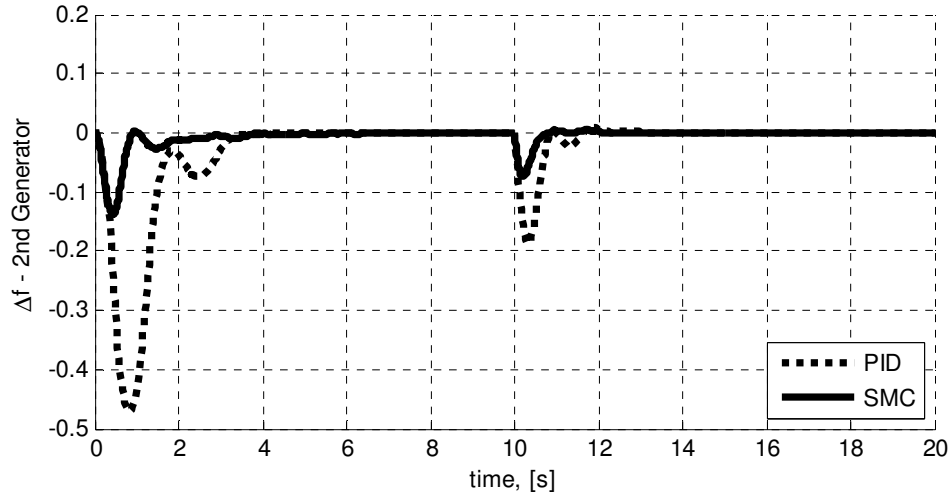

Fig.11. Frequency deviation in 2^{nd} area.

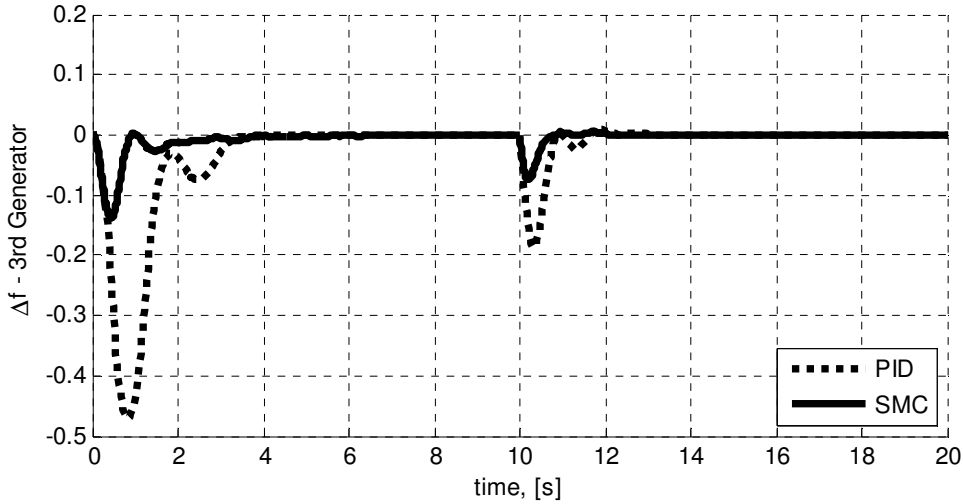

Fig.12. Frequency deviation in 3^{rd} area.

It can be concluded from Fig.10 to 12 that again the implementation of a decentralized SMC compensator improves the performance of the system. In comparison to PID, the SMC controller provides smoother frequency regulation and in addition the undershot is significantly reduced.

5.4. System Case 4

This study is devoted to show the behavior of SMC and PID control over BESS and PV equipped power system. The role of disturbance is played by the PV intermittency in first area, similarly to System Case 2. Simulation results are illustrated in Fig.13 to 15.

It is apparent that SMC outperforms PID equipped system in terms of undershot, however, similarly to the System Case 2 SMC reveals chattering feature which is visible but is muted to acceptable values. At closer analysis, the overshoot in Area 1 has been reduced significantly using SMC.

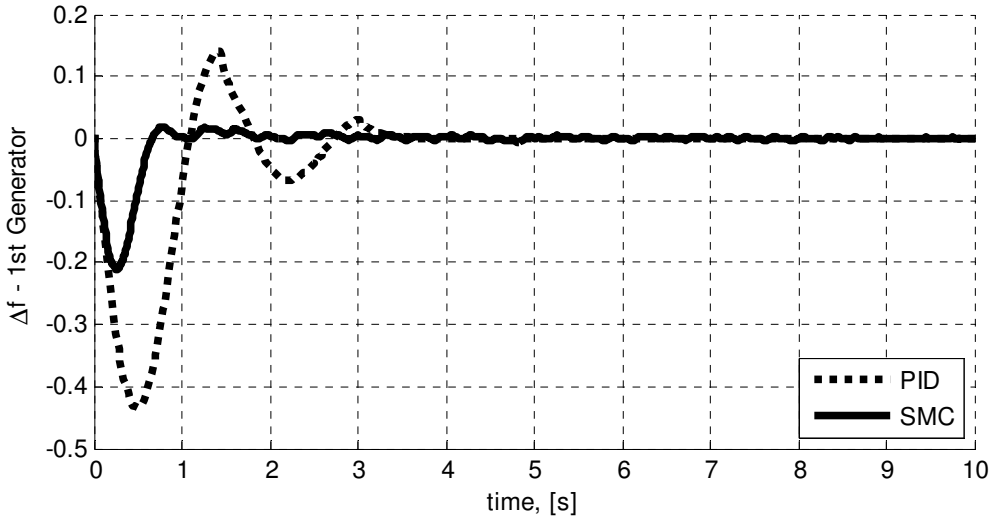

Fig.13. Frequency deviation in 1^{st} area.

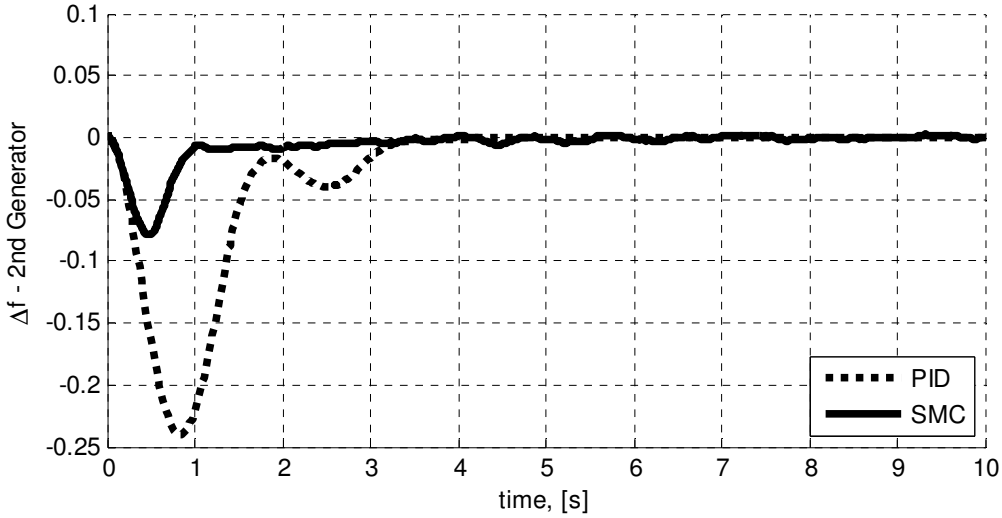

Fig.14. Frequency deviation in 2^{nd} area.

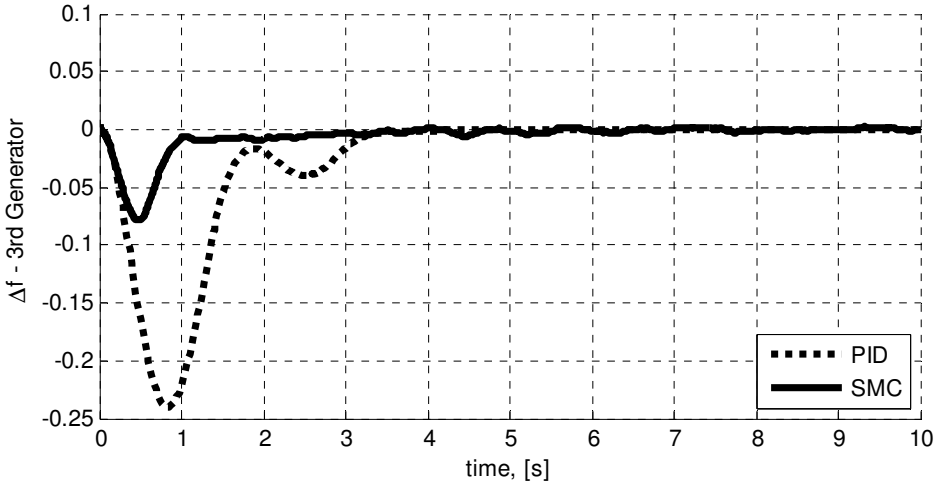

Fig.15. Frequency deviation in 3^{rd} area.

5.5. System Case 5

This test case presents sensitivity analysis of the system equipped with BESS to the PV intermittency. Fig.16 and Fig.17 are frequency responses of the third area to the increasing penetration of PV, namely 25%, 50% and 100%.

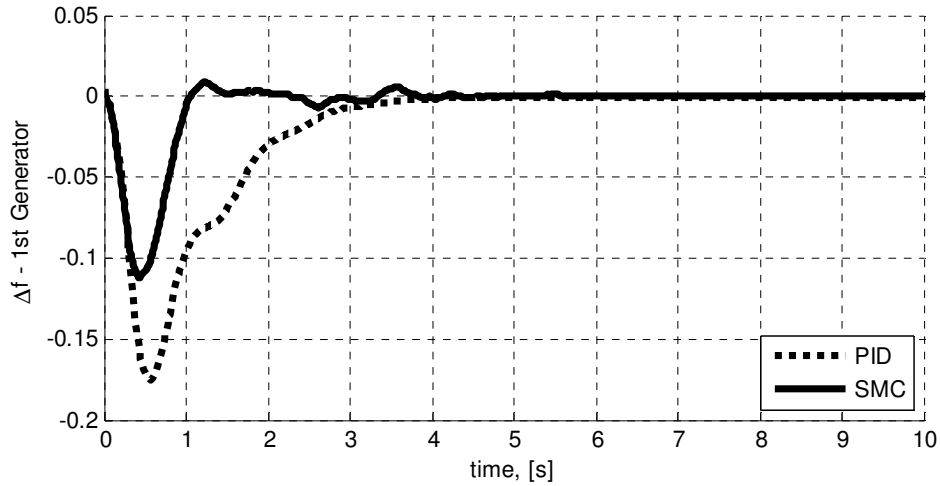

Fig.16. Frequency deviation in 3^{rd} area (25% of PV intermittency).

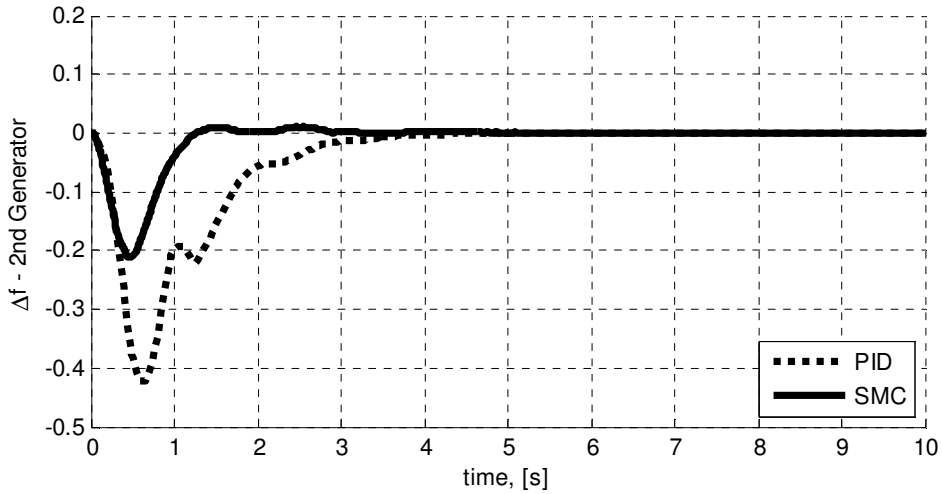

Fig.17. Frequency deviation in 3^{rd} area (50% of PV intermittency).

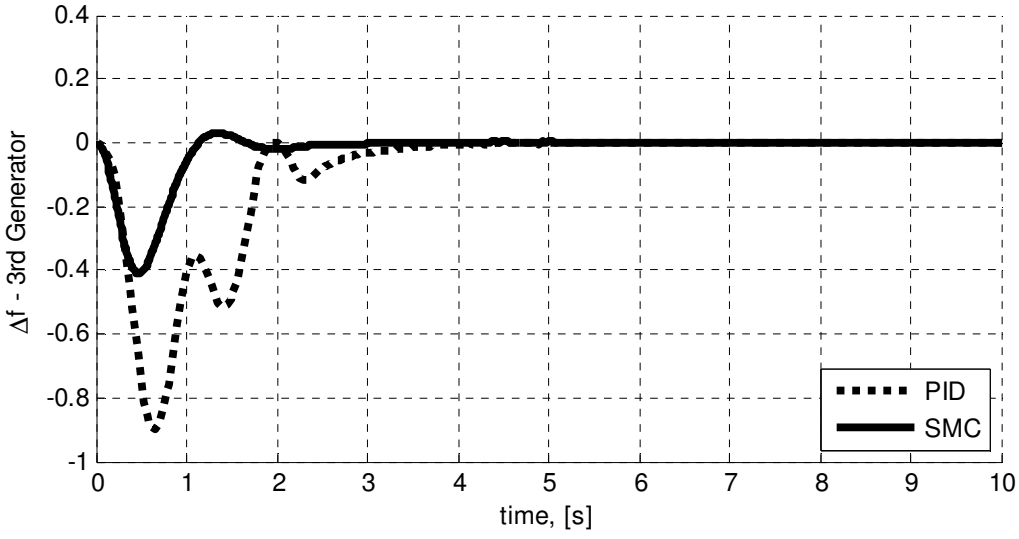

Fig.18. Frequency deviation in 3^{rd} area (100% of PV intermittency).

From the simulation results, it is apparent that the system equipped with SMC is not as vulnerable to change in PV outputs as PID system. In Fig. 18 it has been shown that 100% intermittency of PV has caused severe frequency deviation reaching nearly $-1\ Hz$ while in case of SMC it is still within acceptable limits.

6. Conclusion

This paper is dedicated to demonstrate the SMC for load frequency control problem in multi–area power systems while considering high penetration of DER. For the purpose of this publication three-area power system is chosen. A linear switching surface is chosen to improve the overall frequency stability performance. The influence of SMC is compared to the performance of conventional PID controller. Genetic algorithm has been employed to design the control gains and polynomial coefficients for both secondary frequency regulation strategies. Results indicated that the sliding mode control strategy applied to secondary frequency regulation is more superior to the performance of conventional PID controllers. SMC improves the system frequency responses in term of undershot, smoothness and settling time. Presented simulations reveal chattering issue appearing in some scenarios, however, the switching amplitude is small and finally chattering does not exceed acceptable limits.

Acknowledgment

This work was supported by the Masdar Institute of Science and Technology, research grant no. 13PAMA1

References

[1] Prabha Kundur, Neal J Balu, and Mark G Lauby, Power system stability and control,volume 7, *McGraw-hill New York*, 1994.

[2] *European Network of Transmission System Operators for Electricity*, P1 policy 1: Load-frequency control and performance [c]. June 2004.

[3] Abhijit Chakrabarti and Sunita Halder, Power System Analysis: Operation And Control 3Rd Ed, *PHI Learning Pvt. Ltd*.

[4] Y. Wang, R. Zhou, and C. Wen, New robust adaptive load-frequency control with system parametric uncertainties, *Transmission*, *Generation and Distribution, IEE Proceedings*, 141(3):184–190, May 1994, ISSN 1350-2360, doi: 10.1049/ip-gtd:19949757.

[5] S. Doolla and T.S. Bhatti, Load frequency control of an isolated small-hydro power plant with reduced dump load, *IEEE Transactions on Power Systems*, 21(4):1912–1919, Nov 2006, ISSN 0885-8950, doi: 10.1109/TPWRS.2006.881157.

[6] Yao Zhang, Lili Dong, and Zhiqiang Gao, Load frequency control for multiple-area power systems, *In American Control Conference*, 2009, ACC'09, pages 2773–2778, *IEEE*, 2009.

[7] Xiaofeng Yu and K. Tomsovic, Application of linear matrix inequalities for load frequency control with communication delays, *IEEE Transactions on Power Systems*, 19(3):1508–1515, Aug 2004, ISSN 0885-8950, doi: 10.1109/TPWRS.2004.831670.

[8] D. Rerkpreedapong, A. Hasanovic, and A. Feliachi, Robust load frequency control using genetic algorithms and linear matrix inequalities, *IEEE Transactions on Power Systems*, 18(2):855–861, May 2003, ISSN 0885-8950, doi: 10.1109/TPWRS.2003.811005.

[9] Chun-Feng Lu, Chun-Chang Liu, and Chi-JuiWu, Effect of battery energy storage system on load frequency control considering governor deadband and generation rate constraint, IEEE Transactions on Energy Conversion, 10(3):555–561, Sep 1995, ISSN 0885-8969, doi: 10.1109/60.464882.

[10] A. G. Al-Busaidi, Automatic generation control of the Petroleum Development Oman (PDO) and the Oman Electricity Transmission Company (OECT) interconnected power systems, unpublished phd thesis.
[11] H. Bevrani and P.R. Daneshmand, Fuzzy logic-based load-frequency control concerning high penetration of wind turbines, *IEEE Systems Journal*, 6(1):173–180, March 2012, ISSN 1932-8184, doi: 10.1109/JSYST.2011.2163028.
[12] KA Ellithy and KA El-Metwally, Design of decentralized fuzzy logic load frequency controller, *International Journal of Intelligent Systems and Applications (IJISA)*, 4(2):66, 2012.
[13] H. Bevrani, P.R. Daneshmand, P. Babahajyani, Y. Mitani, and T. Hiyama, Intelligent lfc concerning high penetration of wind power: Synthesis and real-time application, *IEEE Transactions on Sustainable Energy*, 5(2):655–662, April 2014, ISSN 1949-3029, doi: 10.1109/TSTE.2013.2290126.
[14] Z. Al-Hamouz, H. Al-Duwaish, and N. Al-Musabi, Optimal design of a sliding mode fAGCg controller: Application to a nonlinear interconnected model, *Electric Power Systems Research*, 81(7):1403 – 1409, 2011, ISSN 0378-7796.
[15] Yao Zhang, Lili Dong, and Zhiqiang Gao, Load frequency control for multiple-area power systems, *In American Control Conference*, 2009. ACC'09, pages 2773–2778, IEEE, 2009.
[16] D. Rerkpreedapong, A. Hasanovic, and A. Feliachi, Robust load frequency control using genetic algorithms and linear matrix inequalities, *IEEE Transactions on Power Systems*, 18(2):855–861, May 2003, ISSN 0885-8950, doi: 10.1109/TPWRS.2003.811005.
[17] K. Abe, S. Ohba, and S. Iwamoto, New load frequency control method suitable for large penetration of wind power generations, *In Power Engineering Society General Meeting*, 2006, IEEE, pages 6 pp.–, 2006, doi: 10.1109/PES.2006.1709177.
[18] S.K Aditya and D Das, Battery energy storage for load frequency control of an interconnected power system, *Electric Power Systems Research*, 58(3):179 – 185, 2001, ISSN 0378-7796, doi: http://dx.doi.org/10.1016/S0378-7796(01)00129-8.
[19] K. P. Singh Parmar, Load frequency control of multi-source power system with redox flow batteries: An analysis, *International Journal of Computer Applications*, 88(8): 46–52, February 2014.
[20] Ming-Sheng Yang and Hung-Ching Lu, Sliding mode load-frequency controller design for dynamic stability enhancement of large-scale interconnected power systems, 1999, ISIE '99, *Proceedings of the IEEE International Symposium on In Industrial Electronics*, volume 3, pages 1316–1321 vol.3, 1999, doi: 0.1109/ISIE.1999.796894.
[21] Yang Mi, Yang Fu, Chengshan Wang, and Peng Wang, Decentralized sliding mode load frequency control for multi-area power systems, *IEEE Transactions on Power Systems*, 28(4):4301–4309, Nov 2013, ISSN 0885-8950, doi: 10.1109/TPWRS.2013.2277131.
[22] ABB Energy Storage Modules (ESM) for electrical power system scale: http://www05.abb.com/global/scot/scot235.nsf/veritydisplay/f09413974e2f041cc12579e3004fa562/$file/energy_storage_modules_brochure_rev_e.pdf.
[23] V. Utkin, Variable structure systems with sliding modes, *IEEE Transactions on Automatic Control*, 22(2):212–222, Apr 1977, ISSN 0018-9286, doi: 10.1109/TAC.1977.1101446.
[24] Yuri Shtessel, Christopher Edwards, Leonid Fridman, and Arie Levant, Sliding mode control and observation, *Springer*, 2014.
[25] Mitchell, Melanie, An introduction to genetic algorithms, *MIT press*, 1998.
[26] P1 policy 1: Load-frequency control and performance [c], June 2004.
[27] Balancing and frequency control - a technical document prepared by nerc resources subcommittee, 26 January 2011